

## Article

# Metallic Calcium as a Precursor for Sol-Gel Synthesis of CaCO<sub>3</sub>-SiO<sub>2</sub> and CaO-SiO<sub>2</sub> Systems <sup>†</sup>

Piotr Marciniak <sup>1</sup>, Bogna Sztorch <sup>1</sup>, Agnieszka Martyla <sup>1</sup>, Agnieszka Czapik <sup>2</sup>, Mikołaj Stodolny <sup>2</sup> and Robert E. Przekop <sup>1,\*</sup> 

<sup>1</sup> Centre for Advanced Technologies, Adam Mickiewicz University in Poznan, ul. Uniwersytetu Poznanskiego 10, 61-614 Poznan, Poland; piomar12@amu.edu.pl (P.M.); bogna.sztorch@amu.edu.pl (B.S.); agnieszka.martyla@amu.edu.pl (A.M.)

<sup>2</sup> Faculty of Chemistry, Adam Mickiewicz University in Poznan, ul. Uniwersytetu Poznanskiego 8, 61-614 Poznan, Poland; agacz@amu.edu.pl (A.C.); stodolny@amu.edu.pl (M.S.)

\* Correspondence: r.przekop@gmail.com or rprzekop@amu.edu.pl

<sup>†</sup> The article is dedicated to the 80th birthday of Bogdan Marciniak.

**Abstract:** A series of binary oxide systems with Ca/Si molar ratios of 0.05, 0.1, 0.25, 0.5 and 1.0 have been synthesized by the sol-gel technique from tetraethyl orthosilicate (TEOS) and metallic calcium powder. Upon calcination, a side effect of wollastonite formation as a result of the reaction between the components of the material has been observed in the two calcium-richest systems. The increase in calcium content produces an effect of porosity promotion. At high calcium contents, the homogeneity of the systems is limited by the ability of silica to disperse the calcium component. The properties of these systems are determined by the silica surface coverage with a large amount of the scattered CaCO<sub>3</sub> fine microcrystallites (calcite), resulting from the phase segregation. The gels were characterized by X-ray powder diffraction, low temperature nitrogen adsorption, transmission and scanning electron microscopy (TEM, SEM and SEM/EDS), thermogravimetric analysis (TGA), and FT-IR spectra, to describe the parameters important from the point of view of their application as a support for metal-based catalysts.

**Keywords:** sol-gel; metallic precursor; CaO; SiO<sub>2</sub>; one-pot; CaCO<sub>3</sub>; wollastonite



**Citation:** Marciniak, P.; Sztorch, B.; Martyla, A.; Czapik, A.; Stodolny, M.; Przekop, R.E. Metallic Calcium as a Precursor for Sol-Gel Synthesis of CaCO<sub>3</sub>-SiO<sub>2</sub> and CaO-SiO<sub>2</sub> Systems. *Ceramics* **2021**, *4*, 278–290. <https://doi.org/10.3390/ceramics4020022>

Academic Editors: Anna Lukowiak and Gilbert Fantozzi

Received: 20 April 2021

Accepted: 28 May 2021

Published: 4 June 2021

**Publisher's Note:** MDPI stays neutral with regard to jurisdictional claims in published maps and institutional affiliations.



**Copyright:** © 2021 by the authors. Licensee MDPI, Basel, Switzerland. This article is an open access article distributed under the terms and conditions of the Creative Commons Attribution (CC BY) license (<https://creativecommons.org/licenses/by/4.0/>).

## 1. Introduction

Thanks to their chemical and physical properties, silica and calcium oxide are the subject of several studies [1]. They are used in absorption, catalysis, and as highly efficient catalysts obtained by the sol-gel process in the production of biodiesel [2]. The CaO-SiO<sub>2</sub> system also exhibits activity in the retro-aldol reaction for diacetone alcohol production [3]. Many tertiary and quaternary compositions of CaO-SiO<sub>2</sub> with other oxides (P<sub>2</sub>O<sub>5</sub> and Na<sub>2</sub>O) in the form of glasses are known, which, thanks to their biological compatibility, can be combined with human tissues (bone tissue regeneration). These properties are determined both by the composition of such materials and their preparation method [4]. The benefits arising from the use of a sol-gel process allow for the production of glass of a larger surface area and higher purity as compared to traditional methods (melt-casting and grinding) and of greater bioactivity [5–8]. CaO-based systems are useful for hydrogen production from biomass, acting as a CO<sub>2</sub> sorbent. In these processes, CaO-SiO<sub>2</sub> have also been used successfully as an active phase support, increasing the specific surface area and porosity of the metallic catalyst [9]. A Ni-Cu catalyst supported on a CaO-SiO<sub>2</sub> system obtained by the sol-gel method exhibits high conversion and H<sub>2</sub> selectivity in the steam reforming of methanol [10].

A high temperature reaction between CaO and a SiO<sub>2</sub> precursor mixture yields calcium silicate (wollastonite). Porous, synthetic, high mechanical strength wollastonite doped with

hydroxyapatite is a promising biocompatible material for an artificial substituent of bone tissue and for applications in dentistry [11,12].

Instead of a precipitation method, a microwave-assisted solid phase synthesis of wollastonite is also feasible [13].

The bioactive properties of synthetic calcium silicate (wollastonite) activate various processes related to the growth and regeneration of bones and immunomodulation [14,15]. It can be also used as an auxiliary material in tooth restoration with dental implants to assist the regeneration of surrounding tissues [16]. The introduction of  $B_2O_3$  as a sintering additive increases its flexural strength greatly [15]. Wollastonite is a component of glass-ceramic biocompatible materials [17].

Naturally available wollastonite powder can potentially be used to stabilize the soil structure before construction work or other civil engineering work is launched, in order to meet the geotechnical requirements [18]. Its properties make it a good reinforcing filler in composite construction and building materials (e.g., cement) and as an additive in many industrial products [19]. Among other industrial applications, it also shows catalytic activity e.g., in the dehydrogenation of isopropanol to acetone [20].

As opposed to the precipitation method, the proposed synthesis via the sol-gel route is a method of obtaining pure materials with no traces of inorganic admixtures and residual ionic content. It can be extended to other oxide systems.

## 2. Materials and Methods

### 2.1. Materials

Tetraethyl orthosilicate (TEOS, reagent grade, 98%), acetic acid ( $\geq 99.5\%$ ), metallic calcium (powder, max. particle size 400  $\mu\text{m}$ , 99.9%) were purchased from Sigma-Aldrich and used as received, without any further treatment. Water was deionized.

### 2.2. Preparation

$\text{CaCO}_3\text{-SiO}_2$  systems with Ca/Si molar ratios of 0.05, 0.1, 0.25, 0.5 and 1.0 were synthesized by aqueous sol-gel chemistry [21,22]. TEOS was used as a precursor of the starting silica gel, while acetic acid was applied as a main moderator of hydrolysis and condensation rates (regulation of pH). The reaction was performed in a two-liter glass reactor upon stirring under reflux. The silica precursor (100  $\text{cm}^3$ , 94 g of TEOS) was slowly added and hydrolyzed in 700  $\text{cm}^3$  of water at 75  $^\circ\text{C}$  and after 2 h of stirring the resulting slurry was peptized with 29.4 g (28  $\text{cm}^3$ ) of anhydrous acetic acid. In all preparations the molar ratio of TEOS, water and acetic acid was constant and equal to 1:85:1.06. The sol was refluxed for 24 h at 95  $^\circ\text{C}$ . After cooling to room temperature, metallic calcium granules were added stepwise as the second oxide component precursor. The resulting mixture was refluxed upon vigorous stirring for 18 h at 95  $^\circ\text{C}$ . The final product was a homogeneous liquid gel. The gel was poured onto the Petri dishes and dried at 65  $^\circ\text{C}$  for 72 h to obtain a monolithic xerogel used for thermogravimetric analysis. Next, the dry gel was heated at 100  $^\circ\text{C}$  for 12 h, followed by annealing in a tube furnace at 600  $^\circ\text{C}$  for 6 h under air flow. The annealed gel was ground in a mortar and sieved to collect the two required grain fractions, 0.1–0.2 mm and  $<0.1$  mm. For the porous structure determination, the grain size fraction of 0.1–0.2 mm diameter was used (in order to maintain the consistency with the results of our previous studies on similar oxide compositions). For the X-ray powder diffraction (XRPD) and electron microscopy analysis, the latter fraction was used.

Table 1 shows the labeling and composition of the samples, and the amount of calcium in each system (per 100  $\text{cm}^3$  of TEOS).

**Table 1.** Composition and labeling of the studied systems and the amount of metallic calcium added.

| Sample Name                 | SiO <sub>2</sub> | Ca/Si 0.05 | Ca/Si 0.1 | Ca/Si 0.25 | Ca/Si 0.5 | Ca/Si 1.0 |
|-----------------------------|------------------|------------|-----------|------------|-----------|-----------|
| Relative molar amount of Si | 1                | 1          | 1         | 1          | 1         | 1         |
| Relative molar amount of Ca | 0                | 0.05       | 0.10      | 0.25       | 0.50      | 1         |
| Mass of added Ca [g]        | 0                | 0.904      | 1.808     | 4.520      | 9.040     | 18.085    |

### 2.3. Characterization

The samples synthesized in this work were characterized using the following techniques.

#### 2.3.1. X-ray Diffraction Analysis

The X-ray powder diffraction (XRPD) and small angle X-ray scattering (SAXS) measurements were carried out using a Philips PW1050 diffractometer (Poznan, Poland) working in the  $\theta$ - $2\theta$  geometry with Ni-filtered  $\text{CuK}\alpha$  ( $\lambda = 0.15406$  nm) radiation. The following measurement conditions were applied:  $2\theta$  5–100°, voltage 35 kV, current 20 mA, scan step 0.040° at 1° per minute. The SAXS data were directly derived from the XRPD measurements, recalculated in a spreadsheet using the scattering vector formula and presented in a graph.

#### 2.3.2. Thermal Analysis

The thermal transformation of the unprocessed gel samples was carried out on a NETZSCH TG 209 F1 Libra thermogravimetric apparatus (Poznan, Poland). A 5 mg sample was placed in an alumina crucible (85  $\mu\text{L}$  volume) and heated at a rate of 20 °C  $\cdot$  min<sup>-1</sup> to 1000 °C. For all the experiments the fraction of the grain size below 0.1 mm was used. The TG curves were recorded in an air atmosphere with a resolution of 0.1  $\mu\text{g}$ . No drying under vacuum or at an elevated temperature was applied.

#### 2.3.3. SEM, TEM and EDS (Energy Dispersive X-ray Spectroscopy) Analysis

The surface morphology of the oxide gels was depicted by a scanning electron microscope (QUANTA 250 FEG Scanning Electron Microscope (Poznan, Poland)) which was operated in high vacuum conditions at a 5 kV acceleration voltage. The energy dispersive spectroscopy (EDS) analyses were conducted at a beam acceleration voltage of 15 kV using an EDAX Octane SDD detector. EDS maps of elements overlay were made with a resolution of 0.3  $\mu\text{m}$ . TEM analyses were performed using a JEOL 200 CX transmission electron microscope operated at 80 kV.

#### 2.3.4. Porous Structure

The porous structure was determined by the low temperature nitrogen adsorption measurements carried out on an Autosorb iQ Station 2 (Quantachrome Instruments (Poznan, Poland)) in standard analysis mode, using 200–300 mg of material with the grain size fraction between 0.1 and 0.2 mm. Prior to the nitrogen adsorption all samples were outgassed for about 10 h at 350 °C at 0.4 Pa till a constant weight was achieved. Both adsorptive and desorptive branches of the isotherm were taken in the range of  $p/p_0$  0–1. Reports were provided by Quantachrome ASiQwin software (version 2.0). The distribution of pore area and pore volume was calculated using the de Boer t-method and the BJH method. The pore volume and pore diameter were taken from the adsorptive branch of the isotherm using the BJH method. The surface area was calculated using the multi-point BET linear regression method using the  $p/p_0$  0.1–0.3 window and the seven degrees of freedom available (nine data points).

#### 2.3.5. FT-IR Measurements

The FT-IR measurements were carried out using a Thermo Scientific Nicolet iS50 FT-IR spectrometer (Poznan, Poland) in transmission mode. Four mg samples were mixed with 200 mg KBr and pressed at 10 tons pressed into the form of discs. The spectra were recorded using eight scans of background and sixteen scans of sample measurements in the 400–4000  $\text{cm}^{-1}$  using a DTGS detector and a KBr beamsplitter at 0.5 nm resolution.

## 3. Results and Discussion

Table 2 shows the pH values of the gels after the synthesis. With the addition of the calcium component precursor (present in the gel solution as calcium ions), the acidity of the solution decreases continuously in the series of samples to neutral. Only for the Ca/Si

1.0 composition is there an insufficient amount of acid to react with the whole metallic calcium added and the pH value is basic. For that system, approximately 23% of the metallic calcium (remaining after consumption of the whole acetic acid) reacts with water, giving calcium hydroxide that increases the pH value. The pH of the solution changes the net surface charge of the sol particles that depends on the point of zero charge (PZC) of oxide components. Silica particles are charged negatively at a pH higher than the PZC of  $\text{SiO}_2$  ( $\text{pH}_{\text{PZC}} < 4$ , but also values as low as 1.8 were reported [23]) and can attract positively charged calcium species in a basic solution. For the Ca/Si 1.0 system, we assume that the basic pH of the silica solution changes the hydrolysis–condensation reaction ratio and results in a different gel morphology after calcination, consisting of spherical, and not linear particles forming under these conditions.

**Table 2.** Values of pH of the gels after synthesis.

| System Composition | pH   |
|--------------------|------|
| $\text{SiO}_2$     | 3.11 |
| Ca/Si 0.05         | 3.51 |
| Ca/Si 0.1          | 4.24 |
| Ca/Si 0.25         | 5.22 |
| Ca/Si 0.5          | 7.33 |
| Ca/Si 1.0          | 9.24 |

During calcination in air, calcium hydroxide initially present in the freshly synthesized Ca/Si 1.0 system is carbonized to  $\text{CaCO}_3$  with  $\text{CO}_2$  produced during oxidation of organic residues (ethanol from TEOS hydrolysis) and acetone, the formation of which accompanies the thermal decomposition of calcium acetate.

### 3.1. X-ray Powder Diffraction

Presence of some crystalline calcium precursor phase after synthesis that disappears after calcination is visible in X-ray powder diffraction patterns of the Ca/Si dried gels samples shown in Figure 1a. The position of the reflexes differs significantly from the reference patterns of the calcium acetate hydrate, which is caused by differences in the amount of water coordinated to the molecules of calcium acetate [24]. The position of the broad diffraction peak corresponds to the amorphous silica. After the calcination (6 h at 600 °C under oxygen flow) the crystalline calcite phase appears as a result of calcium acetate decomposition (Figure 1b), however its presence is observed in the Ca/Si 0.5 and 1.0 systems only, but with similar intensity. Both these samples show one prominent reflex and a few weak ones originating from wollastonite ( $\text{CaSiO}_3$ ), that may be formed in a reaction between the oxide components of the systems during thermal processing. An amount of crystalline calcium hydroxide phase has been identified in the XRPD pattern of Ca/Si 0.5 system [25], but not in the Ca/Si 1.0 where the presence of a significant amount was expected. This can be explained by the carbonization of  $\text{Ca}(\text{OH})_2$  by the  $\text{CO}_2$  formed as a result of acetone oxidation during calcination in an air atmosphere. Acetone is a product of calcium acetate thermal decomposition.

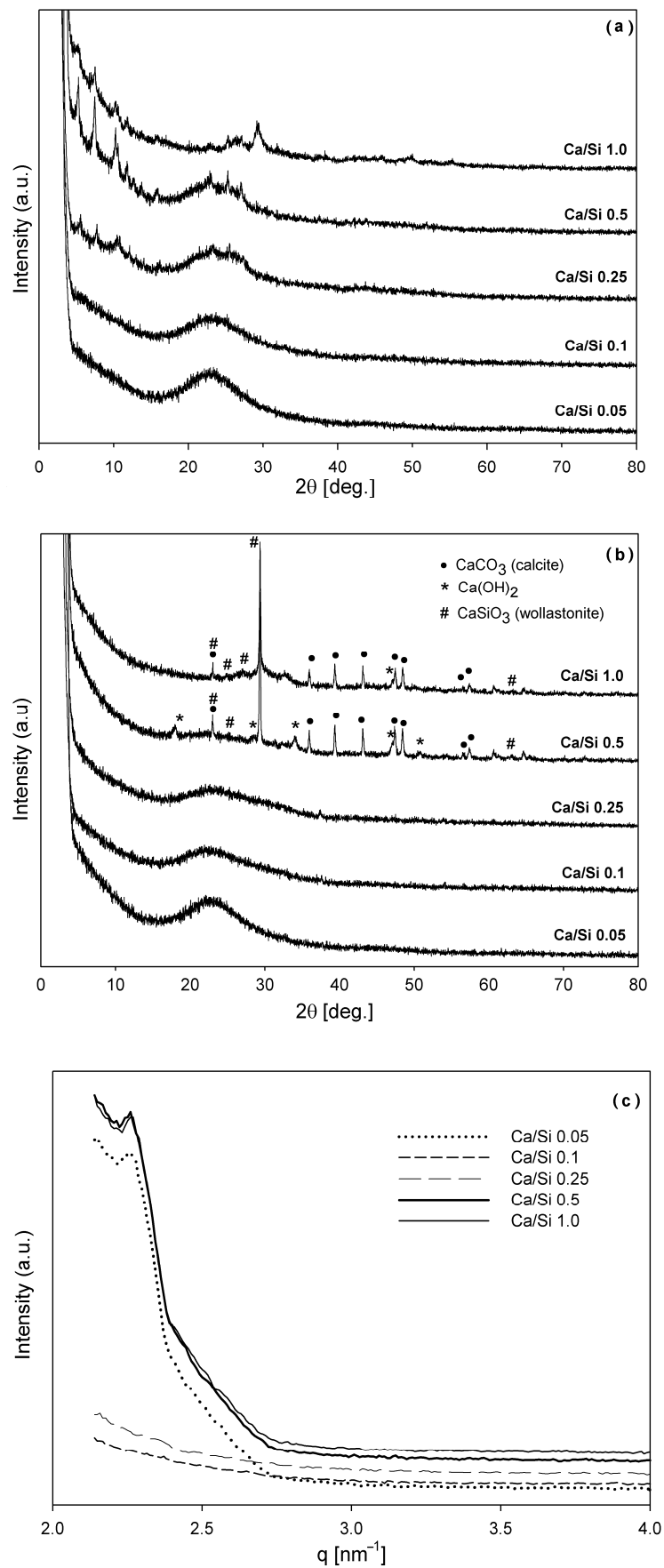


**Figure 1.** XRPD patterns of Ca/Si systems: (a) before calcination; (b) after calcination at 600 °C in oxygen atmosphere; (c) SAXS scattering of calcined samples.

A SAXS intensity profile  $I(q)$  is shown in Figure 1c. The scattering vector  $q$  is given by the formula  $q = (4\pi\sin\theta)/\lambda$ , where  $\theta$  is a measurement angle, and  $\lambda$  is a wavelength of the  $\text{CuK}\alpha$  radiation equal to 0.15406 nm [26].

Both calcined and uncalcined (not shown) samples of Ca/Si 0.5, 1.0 and 0.05 (uncalcined only) gels show strong X-ray scattering on nanometric size particles and pores of these systems. This indicates that the structure of these gels may consist of randomly packed agglomerates of colloidal particles [27] also observed on TEM images formed under more basic conditions (Table 2).

### 3.2. Thermal Analysis

TG and DTG curves of the Ca/Si dry gels recorded under air flow conditions (Figure 2a) are a superposition of the silica gel and calcium acetate hydrate thermograms. For these systems, two characteristic maxima of the thermal effects (at 420–450 °C and 650–750 °C) associated with the transformation of calcium acetate are observed. The first DTG maximum (Figure 2b) is a result of  $\text{CaCO}_3$  formation and the second one corresponds to its decomposition into CaO. The extent of these effects and the total mass loss are proportional to the content of calcium acetate phase in the compositions, and the completeness of these processes at each stage is stated. The maxima of the acetate and carbonate decomposition temperatures increase with the calcium content in the systems. The change of the  $\text{CaCO}_3$  formation temperature over the whole composition range is less than 50 °C, while for its decomposition it is less than 100 °C. For the Ca/Si 0.1 system, the effect of the calcium acetate decomposition is accompanied by an additional overlapping process related probably to some degree of calcium acetate phase inhomogeneity in the silica matrix. At temperatures below 300 °C, the effects of water release from the silica gel structure, silica dehydroxylation and calcium acetate (hydrate) dehydration occur. Table 3 shows quantitative effects of mass loss in the studied Ca/Si systems.

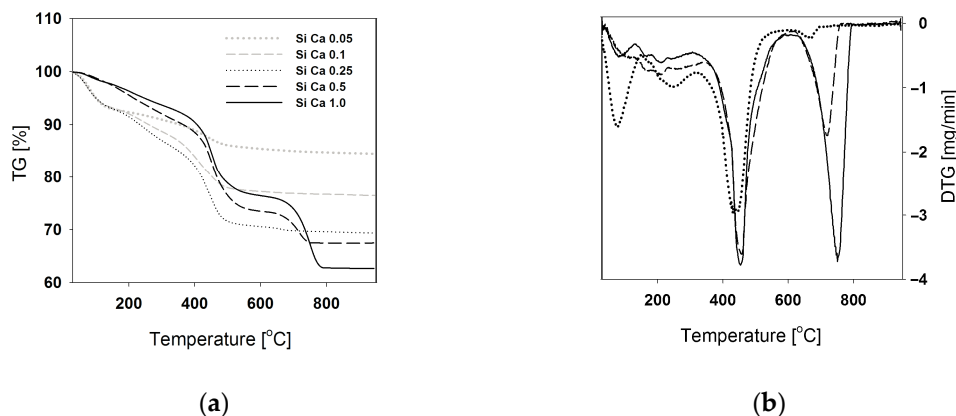


**Figure 2.** Thermogravimetric analysis of Ca/Si systems: (a) TG traces; (b) DTG traces.

The calcium acetate and calcium carbonate decomposition maxima (Figure 2b) are shifted to higher temperatures, compared to the standard samples analyzed under a nitrogen atmosphere, however a part of this effect can also be explained by the dependence of the maxima position on the heating rate, which was relatively high ( $20\text{ °C}\cdot\text{min}^{-1}$ ) for the binary systems.

Significantly lower temperatures of calcium component transformation and decomposition may be a result of its interaction with the silica matrix that provides the dispersion thereof and an effect on its lower particle size. This may be valid with respect to the high surface coverage of the systems with a calcium component, as described in the following paragraph.

At 740–800 °C, the effect of wollastonite formation (Figure 1b) should be observed, but this process has not been registered either on the TG or the DTG curves, even in the systems with the highest Ca content.

**Table 3.** Quantitative mass loss of the Ca/Si systems during thermogravimetric analysis.

| System Composition  | Ca/Si 0.05                  | Ca/Si 0.1       | Ca/Si 0.25 | Ca/Si 0.5 | Ca/Si 1.0 |
|---|-----------------------------|-----------------|------------|-----------|-----------|
| <b>Temperature Range</b>  | <b>Sample Mass Loss [%]</b> |                 |            |           |           |
| I 30–300 °C   | 8.2                         | 11.3            | 12.9       | 7.9       | 6.3       |
| II 300–600 °C   | 6.2                         | 11.5            | 16.5       | 18.6      | 17.2      |
| III 600–800 °C  | 0.9                         | 0.5             | 1.0        | 6.0       | 13.8      |
| Maximum of effect III<br>[°C] (thermal<br>decomposition of<br>CaCO <sub>3</sub> ) | not<br>observed             | not<br>observed | 667        | 727       | 750       |
| Total mass loss [%]   | 15.3                        | 23.3            | 30.3       | 32.5      | 37.3      |

### 3.3. SEM, TEM and EDS Analysis

SEM microscopy provides information on the morphology of the gels after calcination. At a low calcium content (Figure 3a), the gel structure is homogenous and amorphous. The surface is well developed and its texture is wrinkled. The surface of the Ca/Si 1.0 (Figure 3b) is completely covered with a thin layer of randomly distributed calcite crystallites of an approximate length of 2–10 µm and ca. 0.2–0.5 µm width.

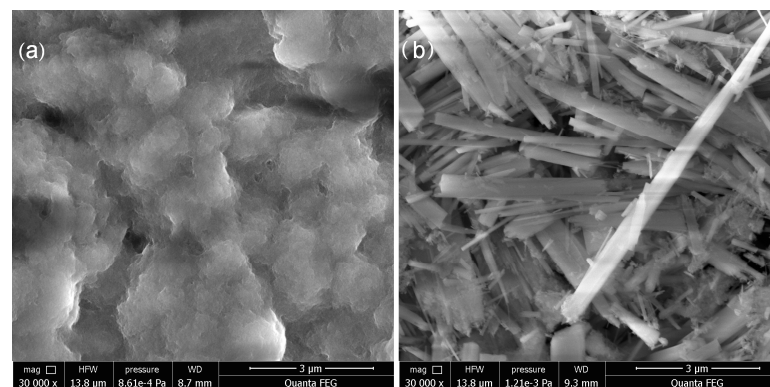


**Figure 3.** SEM micrographs of the systems calcined at 600 °C at the Ca/Si molar ratio: (a) 0.1; (b) 1.0.

TEM images (Figure 4) reveal two different non-uniform silica phases occurring alongside the binary oxides after calcination. One is related to the loose, amorphous silica and the other one consists of highly aggregated, non-spherical, roughly 15–30 nm silica particles. Due to the phase segregation effect, calcium phase particles are not visible at that scale of magnification.

EDS mapping (Figure 5) shows the distribution of the elements at the surface of uncalcined samples of the gels. At low concentration, calcium is dispersed at the surface of silica, but in high concentration this phase is almost completely covering the surface of the silica matrix. The atomic ratio of Ca to Si obtained from the EDS map of Ca/Si 0.1 gel is slightly higher (0.118) than that of the theoretical composition. For the Ca/Si 1.0 gel, the Ca/Si atomic ratio of 13.9 indicates a high degree of the phase segregation in the calcium-rich systems and an increase in the surface coverage with the acetate crystals.

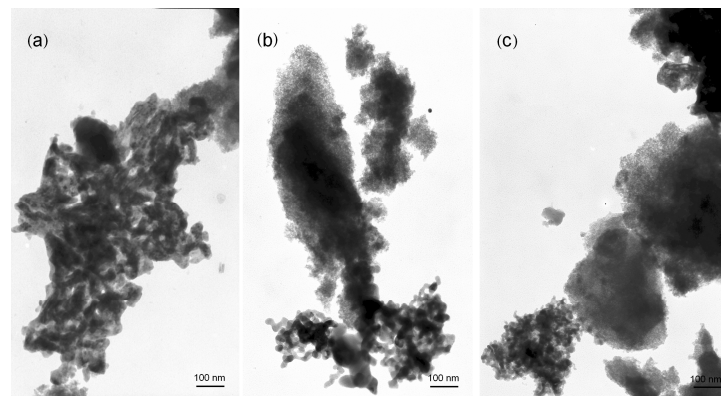


**Figure 4.** TEM micrographs of sol-gel calcined samples at the Ca/Si molar ratio: (a) 0.25; (b) 0.5; (c) 1.0.

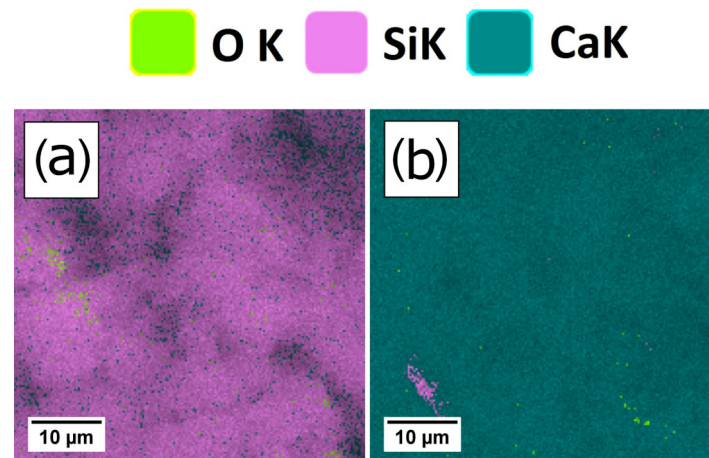


**Figure 5.** SEM-EDS elements maps of Si/Ca systems gel monoliths before calcination at the Ca/Si molar ratio: (a) 0.1; (b) 1.0.

### 3.4. Porous Structure-Low Temperature Nitrogen Adsorption-Desorption

Surface area, pore volume and pore diameter are presented in Table 4. The plots of isotherms, pore volume distribution and pore area distribution are shown in Figure 6.

**Table 4.** Textural properties of Ca/Si systems.

| System Composition | Surface Area $S_{BET}$ [m <sup>2</sup> /g] | Average Pore Diameter $D_{BJH}$ [nm] | Average Pore Volume $D_{BJH}$ [cm <sup>3</sup> /g] |
|--------------------|--|--------------------------------------|--|
| Ca/Si 0.05         | 512  | 3                                    | 0.04   |
| Ca/Si 0.1          | 484  | 3                                    | 0.20   |
| Ca/Si 0.25         | 385  | 3                                    | 0.17   |
| Ca/Si 0.5          | 223  | 5                                    | 0.32   |
| Ca/Si 1.0          | 146  | 13                                   | 0.59   |

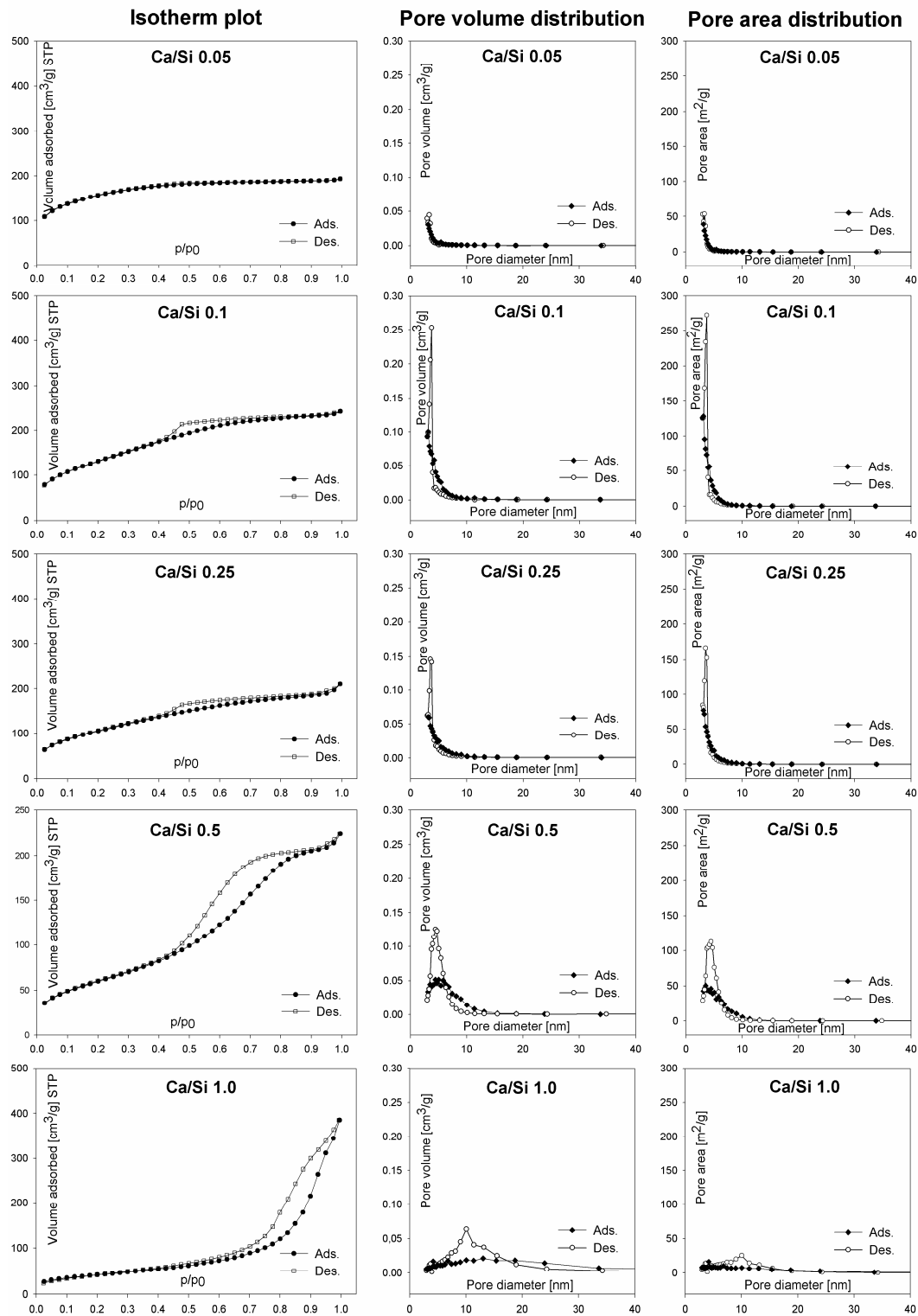


Figure 6. Isotherm, pore volume distribution and pore area distribution of Ca/Si systems.

Binary systems based on SiO<sub>2</sub> with low calcium content have a high initial surface area (~500 m<sup>2</sup>/g) [28], that decreases almost linearly with the increasing content of the latter component. Small mesopores of an average size of approximately 3–4 nm have a major contribution to the surface area and their initial distribution is in a narrow range. Significant amounts of larger mesopores were not found. The low initial pore volume of the binary systems increases with the calcium content in the silica matrix; however, the

pore diameter increases at high calcium content only. The adsorption isotherms are type IV(a) with the H2(b) hysteresis loop (IUPAC) present in the range of the relative pressure  $p/p_0$  0.4–1, characteristic for the mesoporous oxide materials. Unlike the above, the Ca/Si 0.05 system is characterized by the adsorption isotherm of type I(b), which indicates its microporosity [29], or the presence of narrow mesopores. For this system, the highest surface area and lowest pore volume was observed. The pore size distribution of the adsorption (and notably desorption) branch of the isotherms reveals that Ca/Si 0.1 and 0.25 calcined gel samples may be mostly microporous. For the Ca/Si 1.0 composition, the large area of the hysteresis loop is shifted towards higher  $p/p_0$  relative pressure, therefore the prevalence of larger mesopores is typical. It also displays both the highest average volume and diameter of pores in the series, and a relatively high surface area. The morphology of this system is defined by phase segregation and surface enrichment in the calcium component, as evidenced by the SEM observations (Figure 3b).

The Ca/Si 0.5 calcined gel shows transition properties between the two next systems in the series, in terms of isotherms shape, pore volume and area distribution.

For all the compositions based on  $\text{SiO}_2$ , the calcium additive on the surface area and pore volume has a strong effect that is clearly visible in the size and shape of the hysteresis loops. The much smaller effect of the addition of the calcium component on the average diameter of pores was observed, however both the pore volume and diameter increase with calcium content and their distribution broadens as well. This suggests that the total number of the pores increases, while their diameter remains relatively constant.

The decrease in surface area is a result of the diminishing  $\text{SiO}_2$  content that has a dominant contribution to its value. The increase in pore volume and diameter in the subsequent two-component systems can be a result of the  $\text{CaCO}_3$  porosity. It may also be stimulated by the thermal decomposition process of its acetate precursor during calcination, and in the Ca/Si 1.0 system in part by the calcium hydroxide carbonization ( $\text{CO}_2$  from the oxidation of released acetone). The most pronounced impact of the calcium component on the  $\text{SiO}_2$  matrix is visible for the two systems in the series with its highest content, which is caused by morphological differences of these systems resulting from exposition of the calcium carbonate at the surface (Figure 3b). Taking into account the onset position of the adsorption isotherms, it can be concluded that the small mesopores on the silica phase disappear consecutively in the series, which can be explained by their blockage with the calcium component phase, or inaccessibility caused by the surface coverage with calcium carbonate.

### 3.5. FTIR Measurement

Figure 7 shows the FT-IR spectra of the Ca/Si system samples before and after calcination. For both types of the samples, the bands characteristic for the Si-O-Si bonds are visible: symmetric stretching vibrations in the range of  $880\text{--}770\text{ cm}^{-1}$ , asymmetric stretching ( $1100\text{--}1040\text{ cm}^{-1}$ ) and O-Si-O bending modes at  $450\text{--}490\text{ cm}^{-1}$  [27,30] and a  $\text{Ca}(\text{OH})_2$  around  $1790\text{ cm}^{-1}$  band (for uncalcined samples present only in case of Ca/Si 1.0 gel). In the Ca/Si 1.0 system a sharp, intense band of calcium acetate at  $855\text{ cm}^{-1}$ , a band at  $1610\text{ cm}^{-1}$ , a group of bands thereof in the  $700\text{--}600\text{ cm}^{-1}$  region are observed. Uncalcined samples also show characteristic, weak bands of asymmetric and symmetric vibrations of calcium acetate carboxylate groups in the  $1650\text{--}1350\text{ cm}^{-1}$  range. After calcination, as a result of calcium acetate decomposition, these bands disappear and broad, intense bands of symmetric stretching at  $1444\text{ cm}^{-1}$ , bending at  $876\text{ cm}^{-1}$  C-O vibration and  $713\text{ cm}^{-1}$  of calcite [31] and a  $1600\text{--}1680\text{ cm}^{-1}$  bridged bidentate carbonate band appear.

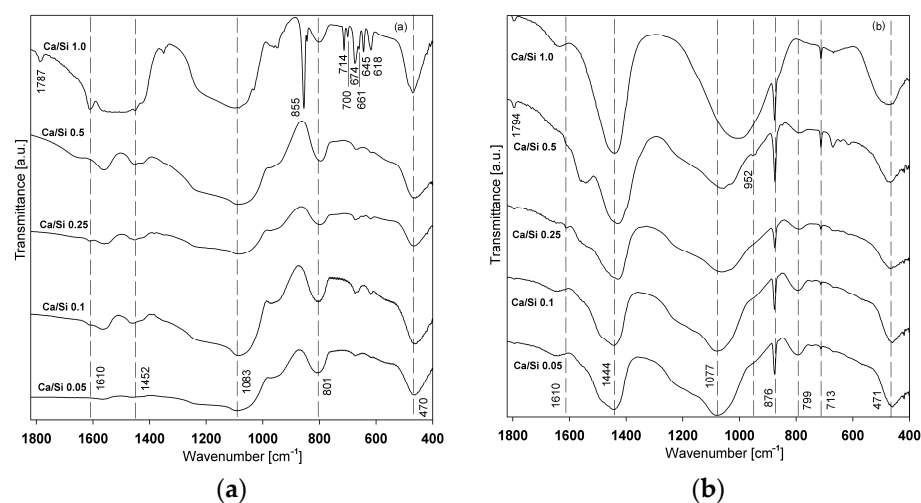


**Figure 7.** FTIR spectra of Ca/Si systems: (a) before calcination, (b) after calcination.

The sharp band at  $876\text{ cm}^{-1}$ , assigned to the ionic carbonate group ( $\text{CO}_3^{2-}$ ) confirms the presence of  $\text{CaCO}_3$  after thermal treatment in the systems [30]. The Si-O-Si asymmetric stretching vibrations around the  $1060\text{--}1090\text{ cm}^{-1}$  band shifts to lower values and overlaps with the  $952\text{ cm}^{-1}$  band of Si-O-Ca bond as the calcium content increases. A similar effect is observed for the Si-O-Si symmetric stretching vibrations around  $799\text{ cm}^{-1}$  but the intensity of that band decreases. The shift of these bands is related to the depolymerization of the silica network [27] and in the former case, to the formation of wollastonite ( $\text{CaSiO}_3$ ).

#### 4. Conclusions

The XRPD data indicate that the structures of the binary Ca/Si systems are mostly amorphous. In some of them, silica is present as an amorphous phase and as its porous agglomerates (Figure 1c). The ability of silica to disperse calcium carbonate in its structure is limited above the Ca/Si 0.25 composition (Figure 1b), and in the system with the highest calcium content this component is also present as a separate microcrystalline calcite phase covering the surface (Figure 3b). For the Ca/Si 0.5 and 1.0 calcined gels, the phase separation and surface excess of the calcium component influence the textural parameters. During the thermal treatment, a small amount of wollastonite is formed in these systems as a result of the reaction between their components.

The high content of  $\text{CaCO}_3$  results in a diminishing of the specific surface area, the value of which the silica has a major contribution. With increasing calcium content, the porosity of the binary systems is enhanced by the  $\text{CaCO}_3$  phase. The narrow pore diameter distribution is broadened and shifted to higher values. The surface area and pore diameter are less affected by the calcium content than the pore volume, that increases over the whole range of the calcium content. In the Ca/Si 1.0 system, the carbonization of calcium hydroxide and its structural transformation to  $\text{CaCO}_3$  during calcination may additionally account for the formation of broad pores. Therefore, for this system, the change in the textural parameters is most pronounced. The calcium component exhibits a high impact on the textural parameters of the calcined gels that include a decrease in microporosity, the promotion of pore formation, a change of surface composition and new phase formation (wollastonite).

The proposed method allows the preparation of high purity materials in a simple way. Depending on the calcination temperature and time, the binary systems of  $\text{CaCO}_3\text{-SiO}_2$  ( $500\text{--}600\text{ }^\circ\text{C}$ ) or  $\text{CaO-SiO}_2$  (above ca.  $800\text{ }^\circ\text{C}$ —note formation of  $\text{CaSiO}_3$  (wollastonite) as well) can be produced while maintaining relatively high textural parameters.

**Author Contributions:** Conceptualization, R.E.P., P.M.; methodology, R.E.P., B.S.; validation, B.S., A.M. and A.C.; formal analysis, M.S., A.C. and A.M.; investigation, B.S., P.M., A.M., M.S., R.E.P. and A.C.; data curation, R.E.P.; writing—original draft preparation, P.M., R.E.P., A.M., A.C. and M.S.; writing—review and editing, P.M., R.E.P., M.S. and B.S.; supervision, P.M. All authors have read and agreed to the published version of the manuscript.

**Funding:** This research received no external funding.

**Institutional Review Board Statement:** Not applicable.

**Informed Consent Statement:** Not Applicable.

**Data Availability Statement:** Not applicable.

**Conflicts of Interest:** The authors declare no conflict of interest.

## References

- Schmetterer, C.; Masset, P.J. Heat capacity of compounds in the CaO-SiO<sub>2</sub> system—A review. *J. Phase Equilib. Diffus.* **2012**, *33*, 261–275. [\[CrossRef\]](#)
- Moradi, G.; Mohadesi, M.; Hojabri, Z. Biodiesel production by CaO-SiO<sub>2</sub> catalyst synthesized by the sol-gel process. *React. Kinet. Mech. Catal.* **2014**, *113*, 169–186. [\[CrossRef\]](#)
- Matsushashi, H.; Kawamura, A. Preparation of a novel solid base catalyst of CaO covered with SiO<sub>2</sub>. *Catal. Today* **2012**, *185*, 236–240. [\[CrossRef\]](#)
- Ebisawa, Y.; Kokubo, T.; Ohura, K.; Yamamuro, T. Bioactivity of CaO-SiO<sub>2</sub> based glasses in vitro evaluation. *J. Mater. Sci. Mater. Med.* **1990**, *1*, 239–244. [\[CrossRef\]](#)
- Li, P.; Ohtsuki, C.; Kokubo, T.; Nakanishi, K.; Soga, N.; Nakamura, T.; Yamamuro, T. Apatite formation induced by silica gel in a simulated body fluid. *J. Am. Ceram. Soc.* **1992**, *75*, 2094–2097. [\[CrossRef\]](#)
- Hench, L.L. Sol-gel materials for bioceramics application. *Curr. Opin. Solid State Mater. Sci.* **1997**, *2*, 604–610. [\[CrossRef\]](#)
- Vallet-Regi, M.; Romero, A.M.; Ragel, C.V.; LeGeros, R.Z. XRD, SEM-EDS, and FTIR studies of in vitro growth of an apatite-like layer on sol-gel glasses. *J. Biomed. Mater. Res. Part A* **1999**, *44*, 416–421. [\[CrossRef\]](#)
- Ungureanu, D.N.; Angelescu, N.; Avram, D.; Catangiu, A.; Bratu, V.; Stoian, E.V. Synthesis, characterization and in vitro bioactivity of SiO<sub>2</sub>-CaO-P<sub>2</sub>O<sub>5</sub> sol-gel glasses highlighted by XRD technique. *Sci. Bull. Valahia Univ. Mater. Mech.* **2011**, *6*, 115–119.
- Zhao, M.; Yang, X.; Church, T.L.; Harris, A.T. Novel CaO-SiO<sub>2</sub> sorbent pectin-cellulose. *Environ. Sci. Technol.* **2012**, *46*, 2976–2983. [\[CrossRef\]](#)
- Yang, R.X.; Chuang, K.H.; Wey, M.Y. Hydrogen production through methanol steam reforming: Effect of synthesis parameters on Ni-Cu/CaO-SiO<sub>2</sub> catalysts activity. *Int. J. Hydrogen Energy* **2014**, *39*, 19494–19501. [\[CrossRef\]](#)
- Papynov, E.; Shichalin, O.; Apanasevich, V.; Portnyagin, A.; Mayorov, V.; Buravlev, I.; Merkulov, E.; Kaidalova, T.; Modin, E.; Afonin, I.; et al. Sol-gel (template) synthesis of osteoplastic CaSiO<sub>3</sub>/HAp powder biocomposite: “in vitro” and “in vivo” biocompatibility assessment. *Powder Technol.* **2020**, *367*, 762–773. [\[CrossRef\]](#)
- Papynov, E.; Shichalin, O.; Modin, E.; Mayorov, V.; Portnyagin, A.; Kobyljakov, S.; Golub, A.; Medkov, M.; Tananaev, I.; Avramenko, V. Wollastonite ceramics with bimodal porous structures prepared by sol-gel and SPS techniques. *RSC Adv.* **2016**, *6*, 34066–34073. [\[CrossRef\]](#)
- Vichaphund, S.; Kitiwan, M.; Atong, D.; Thavorniti, P. Microwave synthesis of wollastonite powder from eggshells. *J. Eur. Ceram. Soc.* **2011**, *31*, 2435–2440. [\[CrossRef\]](#)
- Papynov, E.K.; Shichalin, O.O.; Apanasevich, V.I.; Plekhova, N.G.; Buravlev, I.Y.; Zinoviev, S.V.; Mayorov, V.Y.; Fedorets, A.N.; Merkulov, E.B.; Shlyk, D.K.; et al. Synthetic nanostructured wollastonite: Composition, structure and “in vitro” biocompatibility investigation. *Ceram. Int.* **2021**, in press. [\[CrossRef\]](#)
- Mei, L.; Yin, J.; Xia, Y.; Yao, D.; Liang, H.; Zuo, K.; Zeng, Y.-P. Preparation of high-strength β-CaSiO<sub>3</sub> bioceramic with B<sub>2</sub>O<sub>3</sub> and SiO<sub>2</sub> sintering additives. *Ceram. Int.* **2020**, *46*, 25970–25978. [\[CrossRef\]](#)
- Apanasevich, V.; Papynov, E.; Plekhova, N.; Zinoviev, S.; Kotciurbii, E.; Stepanyugina, A.; Korshunova, O.; Afonin, I.; Evdokimov, I.; Shichalin, O.; et al. Morphological Characteristics of the Osteoplastic Potential of Synthetic CaSiO<sub>3</sub>/HAp Powder Biocomposite. *J. Funct. Biomater.* **2020**, *11*, 68. [\[CrossRef\]](#)
- Mahdy, E.A.; Ahmed, H.Y.; Farag, M.M. Combination of Na-Ca-phosphate and fluorapatite in wollastonite-diopside glass-ceramic: Degradation and biocompatibility. *J. Non Cryst. Solids* **2021**, *566*, 120888. [\[CrossRef\]](#)
- Sai Nikhil, P.; Ravichandran, P.T.; Divya Krishnan, K. Stabilisation and characterisation of soil using wollastonite powder. *Mater. Today Proc.* **2021**, *40*, S161–S166. [\[CrossRef\]](#)
- Zheng, Y.; Wang, C.; Zhou, S.; Luo, C. The self-gelation properties of calcined wollastonite powder. *Constr. Build. Mater.* **2021**, *290*, 123061. [\[CrossRef\]](#)

20. Casas-Luna, M.; Torres-Rodríguez, J.A.; Valdés-Martínez, O.U.; Obradović, N.; Slámečka, K.; Maca, K.; Kaiser, J.; Montúfar, E.B.; Čelko, L. Robocasting of controlled porous CaSiO<sub>3</sub>-SiO<sub>2</sub> structures: Architecture-Strength relationship and material catalytic behavior. *Ceram. Int.* **2020**, *46*, 8853–8861. [[CrossRef](#)]
21. Przekop, R.E.; Marciniak, P.; Sztorch, B.; Czapik, A.; Stodolny, M.; Martyła, A. One-pot synthesis method of SiO<sub>2</sub>-La<sub>2</sub>O<sub>2</sub>CO<sub>3</sub> and SiO<sub>2</sub>-La<sub>2</sub>O<sub>3</sub> systems using metallic lanthanum as a precursor. *J. Non Cryst. Solids* **2019**, *520*, 119444. [[CrossRef](#)]
22. Przekop, R.E.; Marciniak, P.; Sztorch, B.; Czapik, A.; Stodolny, M.; Martyła, A. New method for the synthesis of Al<sub>2</sub>O<sub>3</sub>-CaO and Al<sub>2</sub>O<sub>3</sub>-CaO-CaCO<sub>3</sub> systems from a metallic precursor by the sol-gel route. *J. Aust. Ceram. Soc.* **2018**, *54*, 679–690. [[CrossRef](#)]
23. Kosmulski, M. pH-dependent surface charging and points of zero charge. IV. Update and new approach. *J. Colloid Interface Sci.* **2009**, *337*, 439–448. [[CrossRef](#)]
24. Musumeci, A.W.; Frost, R.L.; Waclawik, E.R. A spectroscopic study of the mineral paceite (calcium acetate). *Spectrochim. Acta Part A* **2007**, *67*, 649–661. [[CrossRef](#)] [[PubMed](#)]
25. García, J.; López, T.; Álvarez, M.; Aguilar, D.H.; Quintana, P. Spectroscopic, structural and textural properties of CaO and CaO-SiO<sub>2</sub> materials synthesized by sol-gel with different acid catalysts. *J. Non Cryst. Solids* **2008**, *354*, 729–732. [[CrossRef](#)]
26. Commissariat à l'énergie atomique et aux énergies alternatives, L'Institut Rayonnement-Matière de Saclay, What is measured in a Small Angle X-ray Scattering (SAXS)? Available online: [http://iramis.cea.fr/Phoceia/Vie\\_des\\_labos/Ast/ast\\_sstechnique.php?id\\_ast=1065](http://iramis.cea.fr/Phoceia/Vie_des_labos/Ast/ast_sstechnique.php?id_ast=1065) (accessed on 5 November 2018).
27. Meiszterics, A.; Rosta, L.; Peterlik, H.; Rohonczy, J.; Kubuki, S.; Henits, P.; Sinko, K. Structural Characterization of Gel-Derived Calcium Silicate Systems. *J. Phys. Chem. A* **2010**, *114*, 10403–10411. [[CrossRef](#)] [[PubMed](#)]
28. Vazquez, N.I.; Gonzalez, Z.; Ferrari, B.; Castro, Y. Synthesis of mesoporous silica nanoparticles by sol-gel as nanocontainer for future drug delivery applications. *Bol. Soc. Esp. Cerám. Vidr.* **2017**, *56*, 139–145. [[CrossRef](#)]
29. Thommes, M.; Kaneko, K.; Neimark, A.V.; Olivier, J.P.; Rodriguez-Reinoso, F.; Rouquerol, J.; Sing, K.S.W. Physisorption of gases, with special reference to the evaluation of surface area and pore size distribution (IUPAC Technical Report). *Pure Appl. Chem.* **2015**, *87*, 1051–1069. [[CrossRef](#)]
30. Pappas, G.S.; Liatsi, P.; Kartsonakis, I.A.; Danilidis, I.; Kordas, G. Synthesis and characterization of new SiO<sub>2</sub>-CaO hollow nanospheres by sol-gel method: Bioactivity of the new system. *J. Non Cryst. Solids* **2008**, *354*, 755–760. [[CrossRef](#)]
31. Kalinkin, A.M.; Kalinkina, E.V.; Zalkind, O.A.; Makarova, T.I. Chemical Interaction of Calcium Oxide and Calcium Hydroxide with CO<sub>2</sub> during Mechanical Activation. *Inorg. Mater.* **2005**, *41*, 1073–1079. [[CrossRef](#)]